MOF Crystallization

DOI: 10.1002/anie.201101757

Kinetic Control of Metal–Organic Framework Crystallization Investigated by Time-Resolved In Situ X-Ray Scattering**

Eli Stavitski, Maarten Goesten, Jana Juan-Alcañiz, Alberto Martinez-Joaristi, Pablo Serra-Crespo, Andrei V. Petukhov, Jorge Gascon,* and Freek Kapteijn*

Metal–organic frameworks (MOFs) are among the most sophisticated nanostructured solids: they often possess high surface areas and pore volumes, with the possibility of fine-tuning their chemical environment by either selecting the appropriate building blocks or by postsynthetic functionalization. For many frameworks, flexibility of the lattice allows them to undergo a significant transformation in solid state.[1] All these features make MOFs a special class of solids with the potential of transcending many common limitations in different technological disciplines, such as ferromagnetism,[2] semiconductivity, gas separation,[3] storage,[4] sensing,[5] catalysis,[6] drug delivery,[7] or proton conductivity.[8] However, the crystallization mechanism of these complex structures is far from understood. Notwithstanding the plethora of publications that present new MOFs,[9] and the effectiveness of the high-throughput approach,[10] serendipity still governs the synthesis of new structures.

Understanding how these materials are assembled will ultimately enable the rational design of new generations of MOFs targeting specific desired topology and properties. Surprisingly, only a small number of crystallization studies on the synthesis of different prototypical MOFs have been reported to date, most notably using X-ray absorption,[11] dynamic light scattering,[12] atomic force spectroscopy,[13] and X-ray diffraction.[14] More recently, Millange and co-workers reported the first in situ diffraction study on the crystallization of different MOFs (CuBTC, MIL-53(Fe), and MOF-14) under hydrothermal conditions.[15] In the latter, the authors emphasized the importance of in situ methods, the necessity of tackling more complex MOF systems, and the use of combined techniques that allow crystallization to be followed over several length scales. The diffraction data provides information about crystalline phases; however, important primary processes, such as reactions occurring in solution or gel formation stages and nucleation, cannot be directly probed.[16,17]

In this work, we report the first in situ combined small- and wide-angle scattering (SAXS/WAXS) study on the crystallization of two topical metal–organic frameworks synthesized from similar metal and organic precursors, NH_2-MIL-101(Al)[18] and NH_2-MIL-53(Al).[19] These two structures differ in the connectivity of the metal nodes and organic linkers: The former contains supertetrahedral (ST) building units formed by aminoterephthalate ligands and trimeric Al^{III} octahedral clusters, whereas the latter consists of $AlO_4(OH)_2$ octahedra connected by the same linker. X-ray scattering was shown to be an indispensible tool for studying the synthesis process of zeolites and zeotypes,[20a–d] mesoporous materials,[20e] nanoparticles and colloids,[20f,g] and interfaces:[20h] This approach is especially valuable when combined with other methods such as XRD, NMR, X-ray absorption, and Raman spectroscopy.[21]

The scattering patterns recorded during the formation of NH_2-MIL-101(Al) at 403 K are shown in Figure 1 a,b. Scattering at low Q (<1 nm^{-1}) develops immediately with the start of the heating well before the formation of most Bragg peaks. The diffraction pattern that was obtained corresponds to the NH_2-MIL-101 structure ($Fd\bar{3}m$, cubic, $a = 88.87$ Å;[18] Figure 1 c). Low Q scattering is likely to be due to the formation of amorphous primary particles which subsequently assemble into the crystalline structures. Remarkably, the reflection at $Q = 6.3$ nm^{-1}, corresponding to a d spacing of 9.7 Å, develops at first. It exhibits a high multiplicity factor of 72: 24 sets of {119} planes and 48 sets of {357} planes contribute to this reflection. From the FWHM of the reflections, the size of the first crystallites was estimated to be about 60 nm in size, reaching about 90 nm after 2500 s. Intensity at low Q remains constant during later phase of the synthesis owing to the cumulative scattering by particles of different sizes and due to scattering by imperfectness of the crystals (such as defects and voids).

Figure 1 d shows normalized crystallization curves produced by integration of the Bragg peak at $Q = 2.4$ nm^{-1} (plane 357) recorded at different temperatures. Analysis of the kinetic profiles was performed using the model developed by Gualtieri[24] and applied for the MOF formation.[15b] This model (see SI) allows decoupling the nucleation and crystal

[*] Dr. E. Stavitski
National Synchrotron Light Source
Brookhaven National Laboratory, Upton, NY 11973 (USA)
E-mail: istavitski@bnl.gov
M. Goesten, J. Juan-Alcañiz, Dr. A. Martinez-Joaristi, P. Serra-Crespo, Dr. J. Gascon, Prof. Dr. F. Kapteijn
Catalysis Engineering—Chemical Engineering Dept
Delft University of Technology
Julianalaan 136, 2628 BL Delft (The Netherlands)
E-mail: j.gascon@tudelft.nl
Homepage: http://www.cheme.tudelft.nl/ce
Dr. A. V. Petukhov
Van't Hoff Laboratory for Physical and Colloid Chemistry
Debye Institute for Nanomaterials Science
Utrecht University (The Netherlands)

[**] We thank ESRF for provision of the beamtime at BM16 beamline, and we are grateful to Dr. François Fauth for his assistance during the use of BM16 beamline. J.G. gratefully acknowledges the Netherlands National Science Foundation (NWO) for a personal VENI grant.

Supporting information for this article is available on the WWW under http://dx.doi.org/10.1002/anie.201101757.

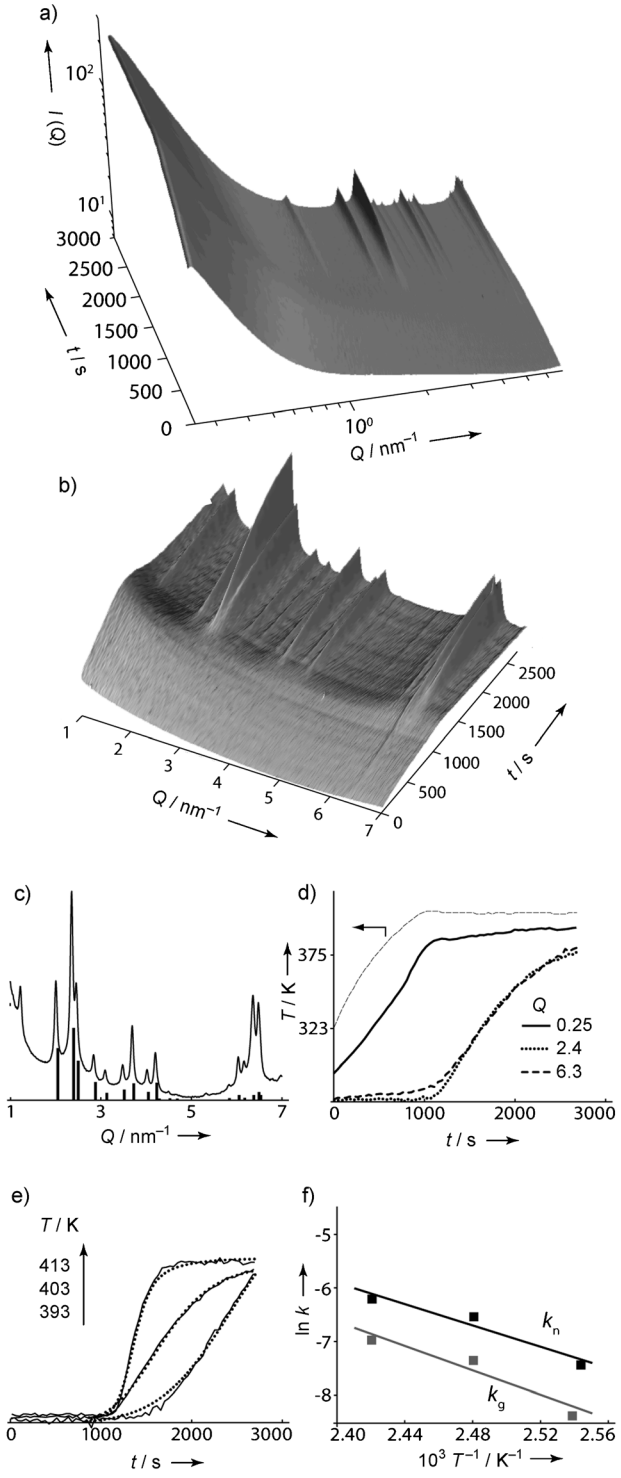

Figure 1. a) 3D SAXS data recorded during crystallization of NH_2-MIL-101(Al) at 403 K using DMF as solvent and low precursor concentrations; b) $Q = 1\text{-}7\ nm^{-1}$ region of (a) focusing on the Bragg reflections; c) SAXS profile taken at 2500 s together with peak positions predicted for NH_2-MIL-101 structure (sticks) calculated from the data from Refs [18, 22]; d) development of the scattering at different Q values. The Bragg peak at $6.3\ nm^{-1}$ emerges earlier than that at $2.4\ nm^{-1}$. Temperature profile in the in situ cell is shown on the left-hand y axis; e) experimental (solid) and calculated (smooth, dotted) profiles of the development of Bragg peak at $Q = 2.4\ nm^{-1}$ recorded at different temperatures. The Gualtieri model was used for kinetic fitting.; f) Arrhenius plots for nucleation and crystal growth rate constants k_g and k_n.

growth processes. The fitting of the kinetic profiles (Figure 1e) yielded nucleation and growth rate constants, k_n and kg, which are given in Table 1. From the Arrhenius plot (Figure 1f), activation energies for nucleation and growth were found to be (82 ± 4) and $(94 \pm 6)\ kJ\,mol^{-1}$ respectively, which is in the range of values reported previously for HKUST-1 and MOF-14.[15b]

Table 1: Crystal growth and nucleation rate constants for NH_2-MIL-101(Al) crystallization extracted from the fitting of experimental profiles recorded at different temperatures.[a]

T [K]	k_g [$10^4\ s^{-1}$]	k_n [$10^4\ s^{-1}$]
393	2.3	5.8
403	6.3	14
413	9.3	20

[a] Syntheses were carried out in DMF with low precursor concentrations. All rate constants are determined with $\pm 10\%$ accuracy.

A conspicuous view of changes in the scattering profile versus time is presented in the Supporting Information, Figure S4, which shows a selection of the $\log Q$–$\log I(Q)$ plots measured in the beginning of the crystallization experiments at 403 K for both NH_2-MIL-101(Al) and NH_2-MIL-53(Al) before the onset of crystallization. In both cases, the SAXS intensity closely follows a power-law decay $Q^{-\alpha}$ with α between 2.9 and 3.2 for NH_2-MIL-101(Al) and between 3.1 and 3.3 for NH_2-MIL-53(Al). In both cases, the decay is slower than the asymptotic behavior of $\alpha = 4$ predicted by the Porod law for compact particles with sharp interfaces,[25] indicating that MOF systems have more complex multiscale structures. SAXS studies of the crystallization of different zeolites yielded α values of about 3,[21b,26] suggesting that the formation of both structures proceeds through a similar precursor gel formation mechanism.

To obtain further insight into the factors governing crystallization, we modified the synthesis conditions. Either increasing the concentration of the precursors or replacing DMF by water as solvent leads to the formation of a different morphology, namely NH_2-MIL-53(Al).[19b] Figure 2a,b shows the scattering patterns obtained during the crystallization process. Similar to the above case, formation of primary particles could be detected from the scattering at low Q, which appears without any detectable induction period (Figure 2a). SAXS data shows development of the Bragg peak at $Q = 6.2\ nm^{-1}$ that is characteristic of NH_2-MIL-53 (I*mma* (no. 74), orthorhombic, $a = 6.9$, $b = 17.6$, $c = 12.1$ Å.[23] It should be noted that owing to the higher concentrations of aminoterephthalic acid and its low solubility, the linker is not dissolved completely in water at room temperature, leading to turbid solutions. This is also manifested in the WAXS patterns (see Figure 2d), where Bragg reflections of the linker can be observed at early times; these features disappear upon dissolution of the linker.

To pinpoint the observed substantial solvent effect, the synthesis of MIL-53 was performed in DMF/water mixtures. As slow dissolution of the linker can significantly hinder the rate of MOF formation, we adjusted the DMF concentration

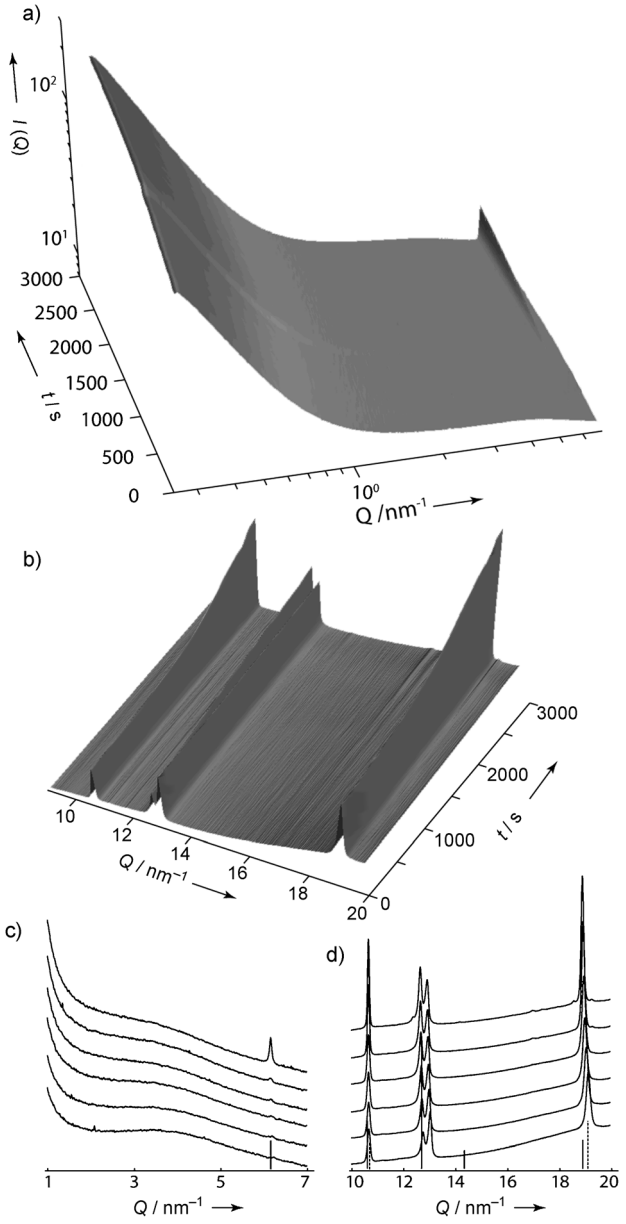

Figure 2. a, b) 3D SAXS (a) and WAXS (b) profiles showing the development of the scattering in the course of NH_2-MIL-53(Al) crystallization at 403 K using water as solvent and high precursor concentrations; c, d) patterns recorded every 200 s, together with the Bragg reflection positions, for NH_2-MIL-53 (solid sticks)[23] and the aminoterephthalic acid linker (dashed sticks). The doublet reflection at $Q = 12.5$–$13\ nm^{-1}$ that overlaps with the Bragg peaks originates from the mica windows (Supporting Information).

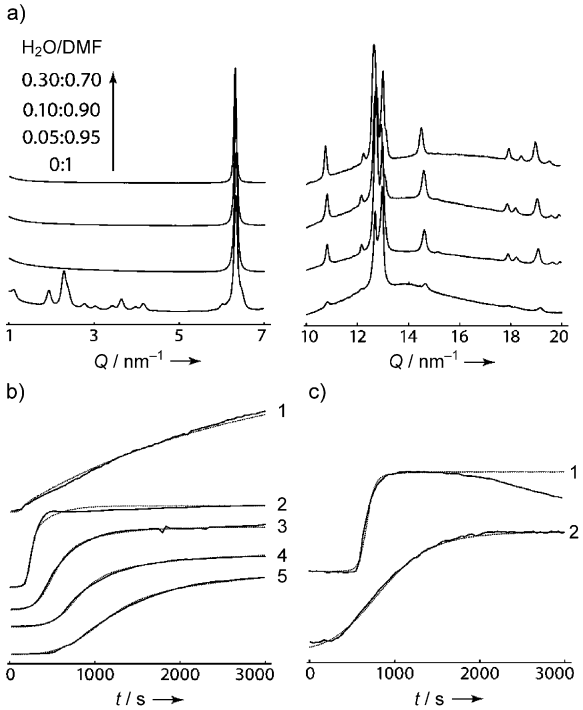

Figure 3. a) SAXS/WAXS profiles taken during crystallization in various solvent mixtures. Note the formation of the MIL-101 phase in DMF; b) temporal development of the MIL-53 Bragg peak at $Q = 6.5\ nm^{-1}$ with H_2O/DMF ratios of 1) 1:0, 2) 0.30:0.70, 3) 0.10:0.90, 4) 0.05:0.95, and 5) 0:1; c) temporal development of the MIL-101 Bragg peak at $Q = 2.3\ nm^{-1}$ in DMF at 1) high and 2) low precursor concentrations. The Gualtieri model was used for kinetic fitting. Note that $t = 0$ for kinetic fitting (smooth lines in (b) and (c)) is chosen when the temperature reaches 90% of the setpoint.

to fully dissolve solid precursors ($DMF/H_2O = 0.70{:}0.30$). This synthesis resulted exclusively in the formation of the MIL-53 framework (Figure 3a). As anticipated, the growth rate constant increased tenfold (Figure 3b and Supporting Information, Table S2), confirming that the availability of linker in solution is critical. The nucleation rate constant remained unchanged and significantly higher than that determined for MIL-101. A further increase of the DMF/water ratio resulted in the decrease of both k_g and k_n. Strikingly, when the synthesis was carried out in DMF, both MIL-53 and MIL-101 phases could be observed.

Inspection of the low Q range (Figure 1a and Figure 2a) shows important differences between MIL-101 and MIL-53 crystallization processes. When development of the scattering intensity is plotted versus time (Supporting Information, Figure S3), scattering at $Q = 0.25\ nm^{-1}$ monotonically increases for all cases, whereas the curves at $Q = 1$ and $1.5\ nm^{-1}$ pass through a maximum in all cases except for the synthesis of MIL-53 in water. Decay in the intensity corresponds to the onset of the MIL-101 Bragg reflection. In terms of local density fluctuations, these findings indicate formation and dissolution of clusters of different sizes. To unveil the chemical nature of these species, we identified a broad Bragg peak at $Q = 6.3\ nm^{-1}$, which appears almost instantaneously with the start of the synthesis (Figure 1b). The structure of a transient phase formed prior to the crystallization of MIL-53(Fe) was reported[15a] and identified as MOF-235,[27] which is composed of iron (III) trimers linked by terephthalate linkers in a similar fashion to the MIL-101 structure. The main Bragg reflection of this structure is predicted to appear at a d spacing of 9.4 Å, corresponding to $Q = 6.3\ nm^{-1}$. Along these lines, we attribute the behavior of the scattering at 1–$1.5\ nm^{-1}$ appearing at early times to the formation of the MOF-235(Al) clusters with sizes in the range

of 4–6 nm and their subsequent dissolution and formation of a more uniform MIL-101 phase.

The above findings enable the major events taking place to be identified during M^{3+}/terephthalate MOF crystallization (Scheme 1). When the linker is completely dissolved, formation of the disordered MOF-235 phase rapidly occurs in the intermediate temperature regime. This phase appears to be kinetically favored. In an aprotic solvent, the assembly of MOF-235 clusters into a MIL-101 phase follows as temperature rises. This is a rate-limiting step, as nucleation rate for MIL-101 is concentration-independent (compare Table 1 and Supporting Information, Table S2 for results at the same temperature). In DMF/water mixtures, MIL-53 crystallization takes place at high temperatures. In the presence of water, MIL-235 phase is hydrolyzed as temperature rises and MIL-53, the thermodynamically favorable phase, is assembled. A larger amount of DMF in the synthesis solution facilitates linker dissolution, increasing availability of the building blocks in the media, and thus favoring the MOF-235. Supporting evidence towards fast formation of the intermediate-phase MOF-235 is the relation between the constants; that is, E_a (growth) > E_a (nucleation) is opposite to that observed for other MOFs.[15b] This implies that in the overall crystallization the end product formation (MIL-101 and/or MIL-53) from MOF-235 is rate-determining. Higher nucleation rate constants (Table 1 and Supporting Information, Table S2) also indicate that crystal growth is the limiting step.

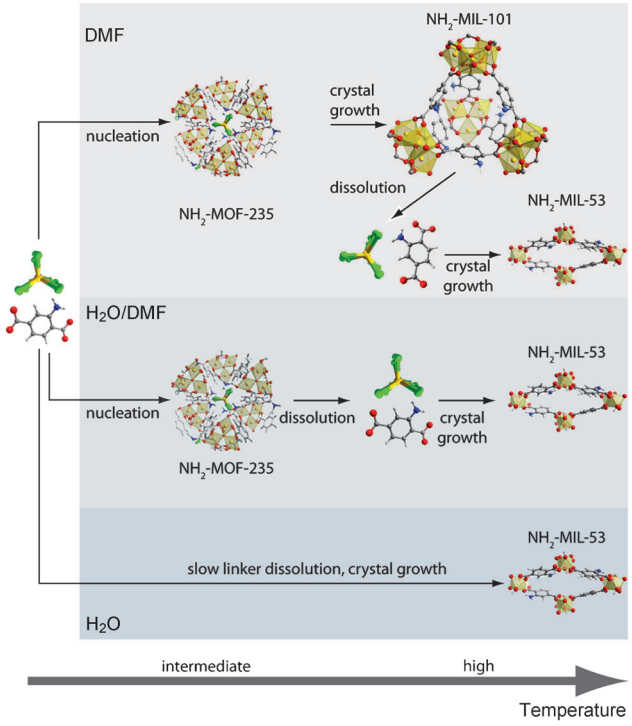

Scheme 1. The sequence of events during the crystallization of terephthalate-based MOFs in different media: Low precursor concentrations (DMF); high precursor concentrations (H_2O/DMF or H_2O). C gray, H white, N blue, O red, Al yellow, Cl green.

To further corroborate involvement of the MOF-235 as the intermediate product, we successfully isolated and characterized this phase quenching the synthesis at intermediate temperatures. The position of the most intense XRD reflection (Supporting Information) agrees with that found in the in situ experiments.

Figure 3c also indicates that at high precursor concentrations, the MIL-101 phase decomposes over time. This observation accentuates that the presence of water formed in the synthesis decreases the stability of this structure. Even when the synthesis is carried out at anhydrous conditions (in DMF), the small amount of moisture introduced with hydrated aluminum salts may suffice to hydrolyze the structure at the synthesis conditions.

To summarize, from the analysis of the X-ray scattering data on different length scales, the chain of events leading to the formation of several MOF phases synthesized from identical precursors has been clarified. Our findings indicate the complexity of the process and the multitude of factors governing the mechanism. It appears that the stabilization of the MOF-235 phase by DMF is essential to the successful synthesis of MIL-101. Notably, this is the first time that this metastable phase has been identified for a metal other than iron. Finally, establishing how synthesis conditions direct the formation of a given topology and how these competing phases are assembled may ultimately permit some fine-tuning of synthesis conditions to test and realize the ideas of design in synthesis, including the synthesis of MOF-based coatings or membranes.[28] As an example, we determined the optimal solvent composition for NH_2-MIL-53 to permit complete linker dissolution: a three-fold increase of product yield was achieved under these conditions (Supporting Information). It should also be emphasized that other methods, such as vibrational spectroscopy and X-ray absorption techniques, should be combined with SAXS/WAXS and also molecular modeling[29] to obtain exhaustive chemical information of the different units assembled during crystallization.

Received: March 11, 2011
Revised: May 13, 2011
Published online: July 14, 2011

Keywords: crystallization kinetics · metal–organic frameworks · MIL-53 · MIL-101 · SAXS/WAXS

[1] G. Férey, C. Serre, *Chem. Soc. Rev.* **2009**, *38*, 1380–1399.
[2] M. Kurmoo, *Chem. Soc. Rev.* **2009**, *38*, 1353–1379.
[3] C. Gucuyener, J. van den Bergh, J. Gascon, F. Kapteijn, *J. Am. Chem. Soc.* **2010**, *132*, 17704–17706.
[4] L. J. Murray, M. Dinca, J. R. Long, *Chem. Soc. Rev.* **2009**, *38*, 1294–1314.
[5] J. R. Li, R. J. Kuppler, H. C. Zhou, *Chem. Soc. Rev.* **2009**, *38*, 1477–1504.
[6] D. Farrusseng, S. Aguado, C. Pinel, *Angew. Chem.* **2009**, *121*, 7638–7649; *Angew. Chem. Int. Ed.* **2009**, *48*, 7502–7513.
[7] P. Horcajada, T. Chalati, C. Serre, B. Gillet, C. Sebrie, T. Baati, J. F. Eubank, D. Heurtaux, P. Clayette, C. Kreuz, J. S. Chang, Y. K. Hwang, V. Marsaud, P. N. Bories, L. Cynober, S. Gil, G. Férey, P. Couvreur, R. Gref, *Nat. Mater.* **2010**, *9*, 172–178.

[8] J. A. Hurd, R. Vaidhyanathan, V. Thangadurai, C. I. Ratcliffe, I. L. Moudrakovski, G. K. H. Shimizu, *Nat. Chem.* **2009**, *1*, 705 – 710.
[9] J. R. Long, O. M. Yaghi, *Chem. Soc. Rev.* **2009**, *38*, 1213 – 1214.
[10] a) R. Banerjee, A. Phan, B. Wang, C. Knobler, H. Furukawa, M. O'Keeffe, O. M. Yaghi, *Science* **2008**, *319*, 939 – 943; b) E. Biemmi, S. Christian, N. Stock, T. Bein, *Microporous Mesoporous Mater.* **2009**, *117*, 111 – 117; c) A. Sonnauer, F. Hoffmann, M. Fröba, L. Kienle, V. Duppel, M. Thommes, C. Serre, G. Férey, N. Stock, *Angew. Chem.* **2009**, *121*, 3849 – 3852; *Angew. Chem. Int. Ed.* **2009**, *48*, 3791 – 3794; d) T. Ahnfeldt, J. Moellmer, V. Guillerm, R. Staudt, C. Serre, N. Stock, *Chem. Eur. J.* **2011**, *17*, 6462 – 6468.
[11] S. Surble, F. Millange, C. Serre, G. Férey, R. I. Walton, *Chem. Commun.* **2006**, 1518 – 1520.
[12] S. Hermes, T. Witte, T. Hikov, D. Zacher, S. Bahnmuller, G. Langstein, K. Huber, R. A. Fischer, *J. Am. Chem. Soc.* **2007**, *129*, 5324 – 5325.
[13] M. Shoaee, M. W. Anderson, M. P. Attfield, *Angew. Chem.* **2008**, *120*, 8653 – 8656; *Angew. Chem. Int. Ed.* **2008**, *47*, 8525 – 8528.
[14] N. A. Khan, S. H. Jhung, *Cryst. Growth Des.* **2010**, *10*, 1860 – 1865.
[15] a) F. Millange, M. Medina, N. Guillou, G. Férey, K. M. Golden, R. I. Walton, *Angew. Chem.* **2010**, *122*, 775 – 778; *Angew. Chem. Int. Ed.* **2010**, *49*, 763 – 766; b) F. Millange, R. El Osta, M. E. Medina, R. I. Walton, *CrystEngComm* **2011**, *13*, 103 – 108.
[16] P. Norby, *Curr. Opin. Colloid Interface Sci.* **2006**, *11*, 118 – 125.
[17] a) P. de Moor, T. P. M. Beelen, R. A. van Santen, L. W. Beck, M. E. Davis, *J. Phys. Chem. B* **2000**, *104*, 7600 – 7611; b) C. J. Y. Houssin, C. E. A. Kirschhock, P. Magusin, B. L. Mojet, P. J. Grobet, P. A. Jacobs, J. A. Martens, R. A. van Santen, *Phys. Chem. Chem. Phys.* **2003**, *5*, 3518 – 3524.
[18] a) P. Serra-Crespo, E. V. Ramos-Fernandez, J. Gascon, F. Kapteijn, *Chem. Mater.* **2011**, *23*, 2565 – 2572; b) J. Juan-Alcañiz, M. Goesten, A. Martinez-Joaristi, E. Stavitski, A. V. Petukhov, J. Gascon, Freek Kapteijn, *Chem. Commun.* **2011**, DOI: 10.1039/c1cc12213d.
[19] a) J. Gascon, U. Aktay, M. D. Hernandez-Alonso, G. P. M. van Klink, F. Kapteijn, *J. Catal.* **2009**, *261*, 75 – 87; b) T. Ahnfeldt, D. Gunzelmann, T. Loiseau, D. Hirsemann, J. Senker, G. Férey, N. Stock, *Inorg. Chem.* **2009**, *48*, 3057 – 3064.
[20] a) S. Y. Yang, A. Navrotsky, D. J. Wesolowski, J. A. Pople, *Chem. Mater.* **2004**, *16*, 210 – 219; b) S. Nikitenko, A. M. Beale, A. M. J. van der Eerden, S. D. M. Jacques, O. Leynaud, M. G. O'Brien, D. Detollenaere, R. Kaptein, B. M. Weckhuysen, W. Bras, *J. Synchrotron Radiat.* **2008**, *15*, 632 – 640; c) T. P. Caremans, B. Loppinet, L. R. A. Follens, T. S. van Erp, J. Vermant, B. Goderis, C. E. A. Kirschhock, J. A. Martens, A. Aerts, *Chem. Mater.* **2010**, *22*, 3619 – 3629; d) S. Kumar, T. M. Davis, H. Ramanan, R. L. Penn, M. Tsapatsis, *J. Phys. Chem. B* **2007**, *111*, 3398 – 3403; e) K. Flodstrom, C. V. Teixeira, H. Amenitsch, V. Alfredsson, M. Linden, *Langmuir* **2004**, *20*, 4885 – 4891; f) G. R. Patzke, Y. Zhou, R. Kontic, F. Conrad, *Angew. Chem. Int. Ed. Angew. Chem. Inter. Ed.* **2011**, *50*, 826 – 859; g) M. Ballauff, *Curr. Opin. Colloid Interface Sci.* **2001**, *6*, 132 – 139; h) D. Grosso, F. Ribot, C. Boissiere, C. Sanchez, *Chem. Soc. Rev.* **2011**, *40*, 829 – 848.
[21] a) C. Aletru, G. N. Greaves, G. Sankar, *J. Phys. Chem. B* **1999**, *103*, 4147 – 4152; b) A. M. Beale, A. M. J. van der Eerden, S. D. M. Jacques, O. Leynaud, M. G. O'Brien, F. Meneau, S. Nikitenko, W. Bras, B. M. Weckhuysen, *J. Am. Chem. Soc.* **2006**, *128*, 12386 – 12387; c) A. Aerts, L. R. A. Follens, M. Haouas, T. P. Caremans, M. A. Delsuc, B. Loppinet, J. Vermant, B. Goderis, F. Taulelle, J. A. Martens, C. E. A. Kirschhock, *Chem. Mater.* **2007**, *19*, 3448 – 3454; d) A. M. Beale, M. G. O'Brien, M. Kasunic, A. Golobic, M. Sanchez-Sanchez, A. J. W. Lobo, D. W. Lewis, D. S. Wragg, S. Nikitenko, W. Bras, B. M. Weckhuysen, *J. Phys. Chem. C* **2011**, *115*, 6331 – 6340.
[22] G. Ferey, C. Mellot-Draznieks, C. Serre, F. Millange, J. Dutour, S. Surble, I. Margiolaki, *Science* **2005**, *309*, 2040 – 2042,.
[23] E. Stavitski, E. A. Pidko, S. Couck, T. Remy, E. J. M. Hensen, B. M. Weckhuysen, J. Denayer, J. Gascon, F. Kapteijn, *Langmuir* **2011**, *27*, 3970 – 3976.
[24] A. F. Gualtieri, *Phys. Chem. Miner.* **2001**, *28*, 719 – 728.
[25] O. Glatter and O. Kratky, *Small Angle X-ray Scattering*, Academic Press, London, **1982**.
[26] D. Grandjean, A. M. Beale, A. V. Petukhov, B. M. Weckhuysen, *J. Am. Chem. Soc.* **2005**, *127*, 14454 – 14465.
[27] A. C. Sudik, A. P. Côté, O. M. Yaghi, *Inorg. Chem.* **2005**, *44*, 2998 – 3000.
[28] a) J. Gascon, S. Aguado, F. Kapteijn, *Microporous Mesoporous Mater.* **2008**, *113*, 132 – 138; b) J. Gascon, F. Kapteijn, *Angew. Chem.* **2010**, *122*, 1572 – 1574; *Angew. Chem. Int. Ed.* **2010**, *49*, 1530 – 1532.
[29] J. Anwar, D. Zahn, *Angew. Chem.* **2011**, *123*, 2042 – 2061; *Angew. Chem. Int. Ed.* **2011**, *50*, 1996 – 2013.

